Auto-selection of quasi-components/components in the multi-dimensional quasi-discrete model

Al Qubeissi, M., Al-Esawi, N. H. I. & Sazhin, S. S.

Original citation & hyperlink:
Al Qubeissi, M, Al-Esawi, NHI & Sazhin, SS 2021, 'Auto-selection of quasi-components/components in the multi-dimensional quasi-discrete model', Fuel, vol. 294, 120245.
https://dx.doi.org/10.1016/j.fuel.2021.120245

DOI 10.1016/j.fuel.2021.120245
ISSN 0016-2361

Publisher: Elsevier

Auto-selection of quasi-components/components in the multi-dimensional quasi-discrete model

Mansour Al Qubeissi[1,2*], Nawar Al-Esawi[1,3], Sergei S. Sazhin[4]

[1]*Institute for Future Transport and Cities, Coventry University, Coventry CV1 5FB, United Kingdom*
[2]*Faculty of Engineering, Environment and Computing, Coventry University, Coventry CV1 2JH, United Kingdom*
[3]*Faculty of Arts, Science and Technology, University of Northampton, Northampton, NN1 5PH, United Kingdom*
[4]*Advanced Engineering Centre, University of Brighton, Brighton BN2 4GJ, United Kingdom*

Abstract

A new algorithm for the auto-selection of quasi-components and components (QC/Cs) in the 'multi-dimensional quasi-discrete' model is suggested. This algorithm is applied to the analysis of heating and evaporation of multi-component fuel droplets. It allows one to automatically select QC/Cs and update the initial selection during droplet evaporation. The new algorithm is expected to be applicable to the analysis of a wide range of fuels and fuel blends. It can be directly implemented into CFD codes with minimal intervention by end-user. Using this algorithm, the effects of transient diffusion of species on droplet lifetimes are investigated for mixtures of Diesel and E85 (85% vol. ethanol and 15% vol. gasoline) fuels. It is shown that the new algorithm can reduce the analysis of the E85-Diesel fuel droplets, taking into account the contributions of up to119 components at the initial stage of heating and evaporation, to that based on 5 QC/Cs, near the end of droplet evaporation, with up to 1.9% errors in predicted droplet temperatures and radii. The CPU time needed to perform calculations using the new algorithm is shown to be 80% less than that when considering the full composition of fuel.

Keywords: Auto-selection algorithm; Evaporation; Fuel blends; Heating; Multi-component fuels; Quasi-components

Nomenclature

Abbreviations

CFD	Computational Fluid Dynamics
CFS	Complex Fuel Surrogates
CPU	Central Processing Unit (in computers)
DC	Discrete Component (model)
E85	Fuel mixture of 85% ethanol and 15% gasoline (volume fraction)
ED	Effective Diffusivity

* Corresponding author: Telephone: +44-(0)2477-658060, E-mail: Mansour.Qubeissi@coventry.ac.uk

ETC	Effective Thermal Conductivity
FACE	Fuel used in Advanced Combustion Engines
MDQD	Multi-Dimensional Quasi-Discrete (model)
QC/Cs	Quasi-Components/ Components
TMDQD	Transient Multi-Dimensional Quasi-Discrete (algorithm)
T.S.	Time Saving
UNIFAC	Universal Quasi-Chemical Functional–group Activity Coefficient

Mathematical Scripts

Symbol	Definition	Units
B_M	Spalding mass transfer number	-
c	Specific heat capacity	$J{\cdot}kg^{-1}K^{-1}$
D	Diffusion coefficient	m^2s^{-1}
d_o	Droplet initial diameter	m (or μm)
G	Group mass fraction	-
h	Convective heat transfer coefficient	$W{\cdot}m^{-2}K^{-1}$
F	Reduction factor in the number of components	-
K	Minimum change in the ratio of group mass fractions	-
k	Thermal conductivity	$W{\cdot}m^{-1}K^{-1}$
L	Latent heat of evaporation	$J{\cdot}kg^{-1}$
$\dot{m}$	Evaporation rate of droplets	$kg{\cdot}s^{-1}$
n	Carbon number	-
N	Number of species	-
Nu	Nusselt number	-
p	Pressure	Pa
p^*	Saturated pressure	Pa
Pr	Prandtl number	-
Pe	Peclet number	-
R	Distance from the droplet centre	m (or μm)
$\dot{R_d}$	Rate of change in droplet radius	$m{\cdot}s^{-1}$
Re	Reynolds number	-
Sc	Schmidt number	-
t	Time	s (or ms)
T	Temperature	K
U	Velocity	$m{\cdot}s^{-1}$
$v_n; v_{nY}$	Eigenfunctions used in Expressions (7), (10) and (11)	-
X	Molar fraction	-
Y	Mass fraction	-

Subscripts

d	Droplet
e	Change due to evaporation
eff	Effective

g	Gas
i	Index of species or their chemical groups
iso	Isolated
j	Index of species forming quasi-components
k	Index of the newly formed QC/Cs
l	Liquid or the numbers of components that form each QC/C (Exprs. (1) and 2))
s	Surface of the droplet
v	Vapour
∞	Far from the droplet surface

Greek Scripts

γ	Activity coefficient	-
ϵ	Relative evaporation rate	-
ε	Minimum ratio of droplet radii	-
κ_R	Effective thermal diffusivity divided by R_d^2	s^{-1}
λ	Eigenvalues in Expressions (7) and (9)	-
μ	Dynamic viscosity	Pa·s
ρ	Density	$kg \cdot m^{-3}$
χ	Correction factors in Expressions (8) and (12)	-
Δ	Relative change	-

1. Introduction

Spray combustion is a complex process, involving two-phase flow, heat and mass transfer in multi-component fuels, and chemical reactions [1,2]. Fuel spray formation in a combustion chamber includes jet break-up into small droplets to form an air-fuel mixture and heating and evaporation of these small droplets. The modelling of these processes is computationally expensive, and not possible without simplification [3]. This difficulty increases when realistic compositions of fuels and their blends, containing hundreds of components, need to be taken into account [4]. Therefore, it is necessary to consider the computational efficiency when developing these models to achieve a balance between computational expense and model accuracy. The treatment of sprays as an array of a large number of spherical droplets is widely accepted [5]. Thus, the analysis of evaporation of sprays can be focused on the analysis of evaporation of isolated individual droplets.

Fuel droplet heating and evaporation are essential thermophysical processes in many engineering applications, including automotive systems [5]. The importance of modelling of these processes has been discussed in many papers (e.g. [6–9]). Fuel droplets, used in engineering applications, are typically complex mixtures of various chemical groups [10]. These groups and their properties need to be considered carefully for accurate simulation of droplet heating and evaporation [11–13]. However, when all fuel components are accounted for (e.g. using the Discrete Component (DC) model; see [14–17] for the details), calculations are likely to be computationally expensive [18]. This problem has been addressed by replacing large numbers of components in fuels with much smaller

numbers of representative components, referred to as 'quasi-components and components' (QC/Cs), in the relatively simple 'quasi-discrete' model [19] and its more advanced version, the 'multi-dimensional quasi-discrete' (MDQD) model [4].

The MDQD model focuses on the analysis of quasi-components (fictitious components with non-integer numbers of atoms) rather than on the actual components used in the DC model. The MDQD model was applied to the analysis of heating and evaporation of droplets of Diesel and gasoline fuels, and their blends with biodiesel and ethanol [4,20–24], and showed substantial improvement in computational efficiency with only a small loss of accuracy. As quasi-components (QCs) used in this model have non-integer carbon numbers, in the general case, their combustion characteristics cannot be described. Also, the choice of QCs in the original version of this model was based on the trial-and error-approach, which made it difficult to implement it into CFD codes. In our most recent study [25], the number of fuel components was reduced via the introduction of representative components using the so-called approximate nearest-integer discrete method. This led to the formulation of Complex Fuel Surrogates (CFS) which were found to be useful in the combustion simulation. As in the original MDQD model, however, the selection of representative components in the CFS model was based on the trial-and-error approach.

This paper focuses on further development of the MDQD model by introducing a new algorithm for automatic selection of quasi-components/components (QC/Cs) during the droplet evaporation process (called TMDQD, where T stands for transient). In the following section, this new algorithm is described. The basic equations of droplet heating and evaporation, used in our analysis, are briefly described in Section 3. The fuel compositions are presented in Section 4. The results of application of the new algorithm to typical fuel droplets are presented in Section 5. In Section 6, the main findings are summarised.

2. Selection algorithm

In the MDQD model, realistic fuel compositions are reduced to a smaller number of quasi-components/components (QC/Cs), with carbon numbers averaged over the groups of individual components with close carbon numbers [4]. In most case, this averaging leads to non-integer carbon numbers, something which is not possible for actual components. These new structures with non-integer carbon numbers are called 'quasi-components'. These quasi-components are treated similarly to the actual components with thermodynamic and transport properties interpolated between those of the components with the nearest integer carbon numbers. For each group of components i (in the case of Diesel fuel, there are 9 such hydrocarbon groups), the carbon numbers of the quasi-components/components (QC/Cs) are calculated as:

$$n_{k_i} = \frac{\sum_{j=J}^{j=J+\ell_{iJ}} (n_j X_j)}{\sum_{j=J}^{j=J+\ell_{iJ}} X_j}. \tag{1}$$

where ℓ_{iJ} are the numbers of components that form each QC/C in group i, for a given value of J; j is the index of the species forming each QC/C in group i in the range J to $J + \ell_{iJ}$, and k_i is the index of the QC/Cs in group i. The numbers ℓ_{iJ} are predefined by the end-user at the initial stage of calculation, based on the initial distribution of species; they do not change during the evaporation process unless species are completely evaporated. The molar fractions of species that form certain QC/Cs are summed up to calculate the molar fractions of those QC/Cs, as follows:

$$X_{k_i} = \sum_{j=J}^{j=J+\ell_{iJ}} X_j, \tag{2}$$

where subscript 'k_i' refers to a specific QC/C in group i.

In contrast to the original application of the MDQD model, the new algorithm does not require direct user involvement in the selection of QC/Cs. Changes in the number of QC/Cs are allowed during the process of droplet heating and evaporation. A flowchart for the new algorithm is shown in Figure 1. Initially (t=0), the number of components is taken equal to the total number of components (i.e. the DC model is used for the prediction of droplet heating and evaporation). Then, during the evaporation process, the formation of QC/Cs is allowed within each group of hydrocarbons, as in the conventional MDQD model. In contrast to the conventional MDQD model, the number of QC/Cs within each group is not pre-selected by the user but is determined by the code at each time-step.

The new algorithm allows automatic reduction of the number of QC/Cs from their initial number to a smaller number, which is determined by the algorithm at specific time-steps. The mass fraction of group i at a certain time-step (G_i) increases or decreases compared with its value in the previous time-step $\left(G_{i_{\text{old}}}\right)$. The species mass fractions are more sensitive to transient effects than their molar fractions; hence, their use in this model to calculate G_i:

$$G_i = \sum_{n=1}^{N_i} Y_{ni}, \tag{3}$$

where Y_{ni} are the mass fractions of individual species n in group i and N_i is the total number of species in the same group i (in the case of Diesel fuel, $N_i \leq 20$ for all groups). The change in G_i is estimated as:

$$\Delta G_i = \frac{\left|G_i - G_{i_{\text{old}}}\right|}{G_i}. \tag{4}$$

If ΔG_i is greater than an *à priori* chosen small number K (in our current analysis, $K = 0.1$), the number of QC/Cs within each group (N_i) is reduced from the previous number $\left(N_{i_{\text{old}}}\right)$ by a certain factor F:

$$N_i = \lceil F\, N_{i_{\text{old}}} \rceil, \tag{5}$$

where F is assumed equal to 0.75, $\lceil\ \ \rceil$ indicates rounding up or down to the nearest integer (e.g. $\lceil 7.5 \rceil$=8 and $\lceil 7.4 \rceil$=7). The number 0.75 is proposed, using a trial-and-error approach, to avoid rapid

reduction in the numbers of QC/Qs at the expense of accuracy for lower F or slow reduction in the numbers of QC/Qs at the expense of computational speed for higher F.

The QCs in our algorithm are formed of the components with the smallest molar fractions in any group i. The selection is based on reverse collation of components to accommodate merging the least contributing components in that group first, starting with the components with the largest carbon numbers (usually the smallest molar fractions) and ending up with the components with the smallest carbon numbers, and usually the highest molar contributions. The number of QC/Cs selected to form the new QCs is taken equal to $\lceil N_i/2 \rceil$. In the case where $\lceil N_i/2 \rceil$ is an even number, the QCs are formed of each 2 components in the half of components with the largest carbon numbers. If $\lceil N_i/2 \rceil$ is an odd number, however, then the nearest component that is not selected is added to this group to form an even number of components and each two QC/Cs in this group are merged to form a new QC. For example, in the case of the alkanes, which include 20 of 98 Diesel fuel components, at the initial stage ($N_{i_{\text{old}}} = 20$), $N_i = \lceil 0 \cdot 75 \times 20 \rceil = 15$ QC/Cs after the first reduction of the number of components. The first 10 components remain unchanged, and the remaining 10 components form 5 QCs (each 2 components form 1 QC). Thus, the averaged carbon numbers of these 5 alkane QCs are determined as:

$$\left.\begin{aligned}
\bar{n}_{(11-12)_{\text{alk}}} &= \left\lfloor \frac{\sum_{j=12}^{j=11} n_j X}{\sum_{j=12}^{j=11} X_j} \right\rfloor \\
\bar{n}_{(13-14)_{\text{alk}}} &= \left\lfloor \frac{\sum_{j=14}^{j=13} n_j X_j}{\sum_{j=14}^{j=13} X_j} \right\rfloor \\
\bar{n}_{(15-16)_{\text{alk}}} &= \left\lfloor \frac{\sum_{j=16}^{j=15} n_j X_j}{\sum_{j=16}^{j=15} X_j} \right\rfloor \\
\bar{n}_{(17-18)_{\text{alk}}} &= \left\lfloor \frac{\sum_{j=18}^{j=17} n_j X_j}{\sum_{j=18}^{j=17} X_j} \right\rfloor \\
\bar{n}_{(19-20)_{\text{alk}}} &= \left\lfloor \frac{\sum_{j=20}^{j=19} n_j X_j}{\sum_{j=20}^{j=19} X_j} \right\rfloor
\end{aligned}\right\}. \tag{6}$$

Similarly, if a certain group contains 11 components, these reduce to $N_i = \lceil 0 \cdot 75 \times 11 \rceil = 8$. The first 5 components remain unchanged, while the last 6 components form 3 QCs – distributed as 2 components each, following the same procedure as shown in (6). The speed of change in mass fractions of certain species or groups is influenced by their high evaporation rates, which indicates the need to reduce their QC/C representation in the fuel composition. When the reduction in group mass fractions G_i is small (i.e. $\Delta G_i \leq K$), the code uses the previous number of QC/Cs, $N_{i_{\text{old}}}$ (i.e. $F = 1$).

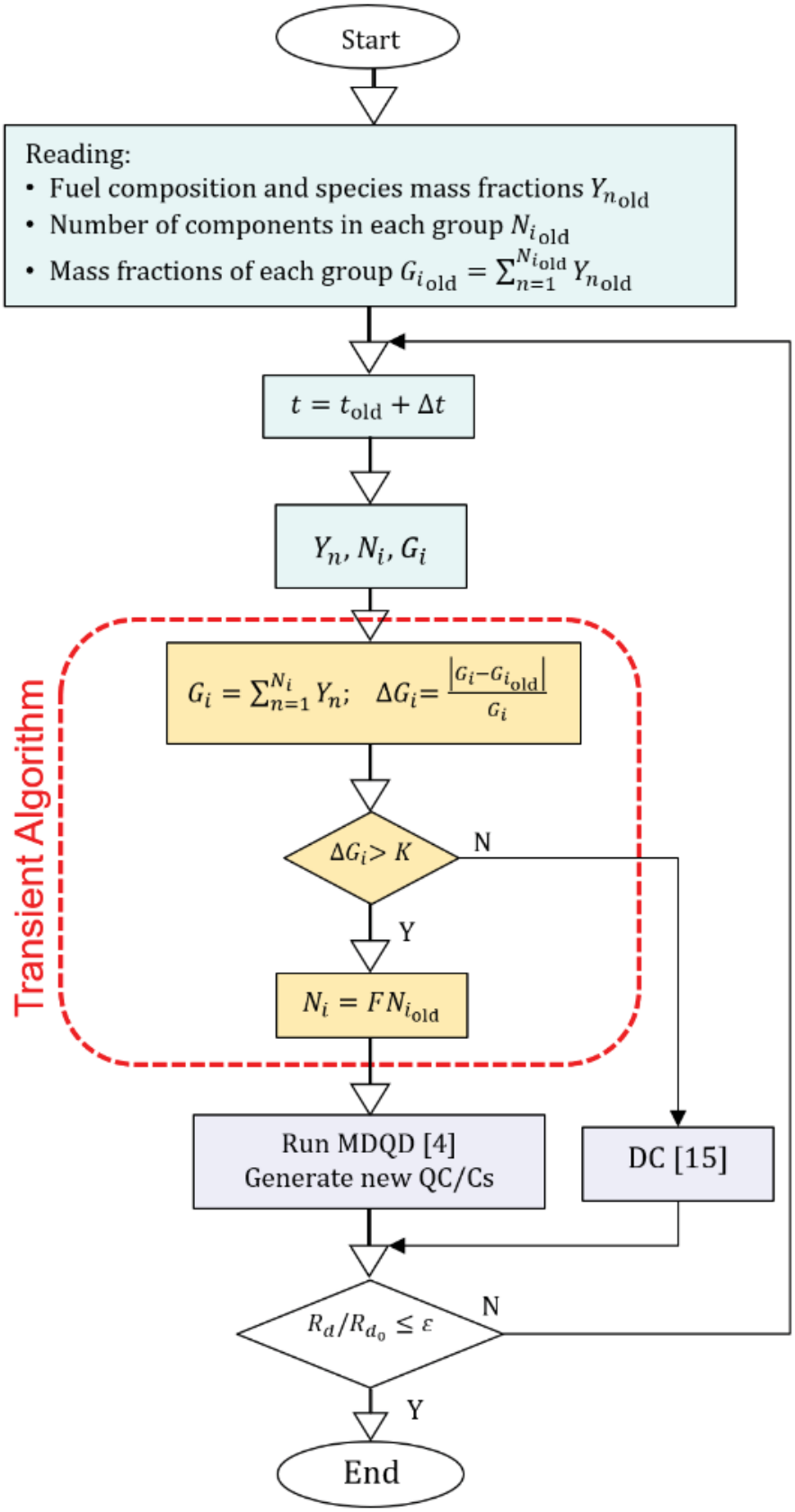

Figure 1. Flowchart of the new algorithm, where the minimum change in mass fraction ratio $K = 0.1$, reduction factor $F = 0.75$ and the minimum ratio of droplet radii $\varepsilon = 10^{-6}$.

In the new algorithm, users can define the minimum number of QC/Cs. This option is built into the final stage of the algorithm when further auto-reduction in the number of QC/Cs is blocked after this

number reaches a certain minimum value. For example, if the minimum number of QC/Cs is defined by the end-user as '10 QC/Cs' and the remaining number of QC/Cs is '15', the auto-reduction will lead to 11 QC/Cs ($\lceil 0.75 \times 15 \rceil$). However, the further reduction of 11 QC/Cs, following the algorithm, would lead to less than 10 QC/Cs. Hence, '11 QC/Cs' will auto-reduce to '10 QC/Cs' only.

The new algorithm can lead to a compromise between the accuracy of the DC model and the computational speed of the original MDQD model. The solution algorithm steps can be summarised as: 1) determine the input parameters for liquid and gas phases, 2) calculate thermodynamic and transport properties at each time-step, 3) update the molar fractions of individual species inside and at the surface of droplets, according to their partial pressures, 4) determine the temperature and mass fractions of species distributions inside the droplet, 5) determine the total evaporation rate and new droplet radius, 6) go to Step 1 if the ratio of droplet radius and the initial droplet radius is greater than an *a priori* chosen number $\varepsilon = 10^{-6}$; otherwise the droplet is assumed to have evaporated.

3. Heating and evaporation model

The discrete component (DC) model is used for the analysis of droplet heating and evaporation [26]. The Effective Thermal Conductivity (ETC) and Effective Diffusivity (ED) models are implemented in this model to take into account the effect of recirculation due to moving droplets [15,27]. The numerical algorithm used in our analysis is based on the analytical solutions to the transient heat conduction and species diffusion equations in the liquid phase, assuming that all processes are spherically symmetric. The following analytical solution for temperature $T = T(t, R)$ at the end of each time-step (t) was used [28]:

$$T(R,t) = \frac{R_d}{R} \sum_{n=1}^{\infty} \left\{ q_n \exp[-\kappa_R \lambda_n^2 t] - \frac{\sin \lambda_n}{\|v_n\|^2 \lambda_n^2} \mu_0(0) \exp[-\kappa_R \lambda_n^2 t] \right\} \sin\left(\lambda_n \frac{R}{R_d}\right) + T_{\text{eff}}(t), \qquad (7)$$

where R is the distance from the centre of the droplet, t is time, $\|v_n\|^2 = \frac{1}{2}\left(1 + \frac{h_{0T}}{h_{0T}^2 + \lambda_n^2}\right)$, $q_n = \frac{1}{R_d \|v_n\|^2} \int_0^{R_d} \tilde{T}_0(R) \sin\left(\lambda_n \frac{R}{R_d}\right) dR$, $\tilde{T}_0(R) = R\, T_{d0}(R)/R_d$, $\kappa_R = \frac{k_{\text{eff}}}{c_l \rho_l R_d^2}$, $\mu_0(t) = \frac{h T_g(t) R_d}{k_{\text{eff}}}$, $h_{0T} = \left(\frac{h R_d}{k_{\text{eff}}}\right) - 1$, c_l is the liquid specific heat capacity and ρ_l is the density of liquid, the positive eigenvalues λ_n ($n > 0$) are determined from $\lambda \cos\lambda + h_{0T} \sin\lambda = 0$. The effective thermal conductivity k_{eff} is defined as:

$$k_{\text{eff}} = \chi k_l, \qquad (8)$$

where k_l is the liquid thermal conductivity, and χ varies between 1 (when Peclet number $\text{Pe}_{\text{d(l)}} = \text{Re}_{d(l)}\text{Pr}_l < 10$) and 2.72 (for $\text{Pe}_{d(l)} > 500$). The model based on Expression (8) is known as the ETC model.

In Expression (7), the effect of droplet evaporation is accounted for using the effective temperature $T_{\text{eff}} = T_g + \frac{\rho_l L \dot{R}_{de}}{h}$, T_g is the ambient (gas) temperature, L is the latent heat of

evaporation, $\dot{R}_{de}$ is the rate of change in droplet radius due to evaporation and $h = \mathrm{Nu}\, k_g/2R_d$ is the convective heat transfer coefficient, based on the Nusselt number (Nu) and the thermal conductivity of air (k_g).

The analytical solution to the equation for mass fractions of species i inside droplets was used [29]:

$$Y_{li} = \epsilon_i + \frac{1}{R}\begin{Bmatrix} \left[\exp\left[D_{\mathrm{eff}}\left(\frac{\lambda_{0Y}}{R_d}\right)^2 t\right][q_{i0} - \epsilon_i Q_0]\sinh\left(\lambda_{0Y}\frac{R}{R_d}\right) + \\ \sum_{\mathrm{n=1}}^{\infty}\left[\exp\left[-D_{\mathrm{eff}}\left(\frac{\lambda_{nY}}{R_d}\right)^2 t\right][q_{in} - \epsilon_i Q_n]\ \sin\left(\lambda_{nY}\frac{R}{R_d}\right)\right] \end{Bmatrix}, \tag{9}$$

where $\epsilon_i = \frac{Y_{vis}}{\sum_i Y_{vis}}$, λ_{0Y} and λ_{nY} are calculated from $\tanh\lambda_{0Y} = -\lambda_{0Y}/h_{0Y}$ and $\tan\lambda_{nY} = -\lambda_{nY}/h_{0Y}$ (for $n \geq 1$), respectively, $h_{0Y} = -\left(1 + \frac{\alpha R_d}{D_{\mathrm{eff}}}\right)$, $\alpha = -\dot{m}_d/(4\pi\rho_{\mathrm{l}}R_d^2)$,

$$Q_n = \begin{cases} -\frac{1}{\|v_{oY}\|^2}\left(\frac{R_d}{\lambda_{0Y}}\right)^2(1+h_{0Y})\sinh\lambda_{0Y} & \text{when } n = 0 \\ \frac{1}{\|v_{nY}\|^2}\left(\frac{R_d}{\lambda_{nY}}\right)^2(1+h_{0Y})\sin\lambda_{nY} & \text{when } n \geq 1 \end{cases}, \tag{10}$$

$$q_{in} = \begin{cases} \frac{1}{\|v_{0Y}\|^2}\int_0^{R_d} R\, Y_{li0}(R)\sinh\left(\lambda_{0Y}\frac{R}{R_d}\right)dR & \text{when } n = 0 \\ \frac{1}{\|v_{nY}\|^2}\int_0^{R_d} R\, Y_{li0}(R)\sin\left(\lambda_{nY}\frac{R}{R_d}\right)dR & \text{when } n \geq 1 \end{cases}, \tag{11}$$

$\|v_{0Y}\|^2 = -\frac{R_d}{2}\left(1 + \frac{h_{0Y}}{h_{0Y}^2 - \lambda_{0Y}^2}\right)$, $\|v_{nY}\|^2 = \frac{R_d}{2}\left(1 + \frac{h_{0Y}}{h_{0Y}^2 + \lambda_{nY}^2}\right)$ $(n \geq 1)$, D_{eff} is the effective diffusivity, defined as:

$$D_{\mathrm{eff}} = \chi_Y D_l, \tag{12}$$

D_l is the liquid diffusion coefficient, χ_Y is calculated as $\chi_{\mathrm{Y}} = 1.86 + 0.86\tanh\left[2.225\log_{10}\left(\mathrm{Re}_{\mathrm{d}(l)}\mathrm{Sc}_l/30\right)\right]$. The model based on Expression (12) is known as the ED model.

The droplet evaporation is calculated using the following expression:

$$\dot{m}_d = -2\pi R_d D_v \rho_{\mathrm{total}} B_M \mathrm{Sh}_{\mathrm{iso}}, \tag{13}$$

where D_v is the binary diffusion coefficient of vapour in gas (air), $\rho_{\mathrm{total}} = \rho_g + \rho_v$ is the total density of the mixture of vapour and ambient gas, $\mathrm{Sh}_{\mathrm{iso}}$ is the Sherwood number for an isolated droplet in which the effects of droplet motion and evaporation are considered, using the Abramzon and Sirignano model [7], $B_M = \frac{Y_{vs} - Y_\infty}{1 - Y_{vs}}$ is the Spalding mass transfer number, and Y_{vs} and Y_∞ are total vapour mass fractions in the vicinity of the droplet surface and in the far-field, respectively, $Y_{vs} = \sum_i Y_{vis}$, Y_{vis} are the vapour mass fractions of individual species i, calculated from the vapour molar fractions at the surface of droplet (X_{vis}), as:

$$X_{vis} = \gamma_i \frac{X_{is}\, p_{vis}^*}{p}, \tag{14}$$

where, X_{is} is the molar fraction of the i^{th} species at the surface of the droplet, γ_i is the activity coefficient of the i^{th} species, p^*_{vis} is the saturated pressure of individual species, and p is the ambient pressure. The DC model used in our analysis was verified in [30] and validated in [22,31]. Following [21,32], the activity coefficient was calculated, using the multi-component universal quasi-chemical functional group activity coefficients (UNIFAC) model [33,34].

4. Fuel composition

Diesel fuel, as described in [4], and gasoline fuel as used in advanced combustion engines – type C (FACE C), are used in our analysis to illustrate the efficiency of the new algorithm. The Diesel fuel used in [4] includes 98 hydrocarbon components, with the following groups and molar fractions: alkanes (40.0556%), cycloalkanes (14.8795%), bicycloalkanes (7.6154%), alkylbenzenes (16.1719%), indanes & tetralines (9.1537%), naphthalenes (8.6773%), tricycloalkanes (1.5647%, represented by the characteristic component $C_{19}H_{34}$), diaromatics (1.2240%, represented by the characteristic component $C_{13}H_{12}$), and phenanthrenes (0.6577%, represented by the characteristic component $C_{14}H_{10}$). The details of this composition are shown in Table 1.

Table 1. Molar fractions (%) of Diesel fuel components, excluding the characteristic components [4].

Carbon no	alkanes	cycloalkanes	bicycloalkanes	alkylbenzenes	indanes & tetralines	naphthalenes
C8	0.308	-	-	0.497	-	-
C9	3.032	-	-	3.2357	-	-
C10	5.0541	0.6408	0.6926	5.3584	1.3157	1.9366
C11	3.163	1.8745	1.0524	0.9492	1.3632	2.5290
C12	2.6156	1.6951	0.9753	1.9149	1.1951	1.4012
C13	2.5439	1.2646	0.6611	0.6873	1.0652	0.7692
C14	2.6497	1.3633	0.5631	0.6469	0.8406	0.4879
C15	3.1646	1.2353	0.4314	0.4782	0.7051	0.3843
C16	2.6579	1.0449	0.4921	0.4564	0.6684	0.2854
C17	2.8605	1.0162	0.6529	0.4204	0.5598	0.2072
C18	3.2403	1.2848	0.6554	0.5234	0.5357	0.2358
C19	3.5296	1.3566	0.9901	0.3226	0.3403	0.2151
C20	2.2338	0.9961	0.1965	0.2848	0.3227	0.2256
C21	1.443	0.5374	0.0935	0.2032	0.1638	-
C22	0.799	0.304	0.0701	0.0969	0.0781	-
C23	0.3972	0.109	0.0488	0.0494	-	-
C24	0.1903	0.0755	0.0234	0.0473	-	-
C25	0.0997	0.0445	0.0169	-	-	-
C26	0.0425	0.0214	-	-	-	-
C27	0.0309	0.0155	-	-	-	-
Total %	40.65	14.88	7.62	16.17	9.15	8.68

The composition of FACE C gasoline fuel is inferred from [23] and includes the following groups and molar fractions: n-alkanes (28.61%), iso-alkanes (65.19%), alkylbenzene (4.25%), indanes (0.10%, represented by its characteristic component C_9H_{10}), cycloalkanes (1.49%, represented by its characteristic component C_8H_{16}), and olefins (0.35%, represented by its characteristic component C_9H_{18}). The details of this composition are shown in Table 2.

Table 2. Molar fractions (%) of gasoline fuel components [23].

Carbon no	n-alkanes	iso-alkanes	alkylbenzenes	cycloalkanes	indanes	olefins
C4	3.905	0.092	-	-	-	-
C5	13.87	7.456	-	-	-	-
C6	10.842	2.98	-	-	-	-
C7	-	11.67	-	-	-	-
C8	-	42.17	0.242	1.49	-	-
C9	-	0.137	3.521	-	0.104	0.346
C10	0.01	0.36	0.44	-	-	-
C11	-	0.113	0.055	-	-	-
C12	0.012	-	-	-	-	-
Total%	28.64	64.98	4.26	1.49	0.104	0.346

Bioethanol free from water (anhydrous) is used in our study (described as 'ethanol') for the fuel mixtures. As in our previous study [22] we assume that ethanol is completely homogeneously spread in Diesel and gasoline fuel mixtures (this is a crude assumption where the mass fraction of ethanol/Diesel is high, due to the differences in their chemical characteristics and structures [35,36]). The following volume fractions of E85 (85% vol. ethanol and 15% vol. gasoline)/Diesel fuel blends are considered in this analysis: pure Diesel (98 hydrocarbons), E85-5 (5% vol. E85 and 95% vol. Diesel) (119 components, comprising 98 Diesel hydrocarbons, 20 gasoline hydrocarbons and 1 ethanol), E85-20 (20% vol. E85 and 80% vol. Diesel) (119 components), E85-50 (50% vol. E85 and 50% vol. Diesel) (119 components), and E85 (21 components, comprising 20 gasoline hydrocarbons and 1 ethanol). The thermodynamic and transport properties of gasoline, Diesel and ethanol are inferred from [4,22,23].

The liquid properties are calculated at the average droplet temperature $\left(T_{av} = \frac{3}{R_d^3}\int_0^{R_d} R^2 T(R)\,\mathrm{d}R\right)$. The vapour properties are calculated at the reference temperature $\left(T_r = \frac{2}{3}T_s + \frac{1}{3}T_g\right)$. The density of gas (air) is calculated using the ideal gas law. The saturated vapour pressure and latent heat of evaporation are calculated at the droplet surface temperature T_s.

5. Results

The new algorithm was used for modelling the heating and evaporation of droplets of Diesel fuel and its E85 fuel blends. Following [21], the initial droplet diameter was taken equal to $d_o = 25.32\ \mu$m; the droplet velocity was assumed constant and equal to $U_d = 10\ \mathrm{m.s^{-1}}$. The initial droplet

temperature was assumed equal to $T_0 = 298$ K. The ambient air pressure and temperature were assumed to be constant and equal to $p_g = 30$ bar and $T_g = 800$ K, respectively.

The evolutions of pure Diesel fuel droplet surface temperatures and radii predicted using the DC model, the original MDQD model and the new algorithm, are presented in Figures 2-3. Five cases are shown: the contributions of all 98 components are considered, using the DC model (indicated as DC (98)); the 98 components are reduced to 15 QC/Cs, using the original MDQD model (indicated as MDQD (15)); the 98 components are reduced to 10 QC/Cs, using the original MDQD model (indicated as MDQD (10)); the 98 components are auto-reduced to 15 (or 10) QC/Cs using the new algorithm (indicated as TMDQD (98-15 (or 98-10)). The application of the TMDQD (98-15 (98-10)) led to 74 QC/Cs (i.e. the nearest integer to 98×0.75) at time instant 0.300 ms, 56 QC/Cs (i.e. $\lceil 74 \times 0.75 \rceil$) at time-instant 0.450 ms, 42 QC/Cs (i.e. $\lceil 56 \times 0.75 \rceil$) at time-instant 0.599 ms, 32 QC/Cs (i.e. $\lceil 0.75 \times 42 \rceil$) at time-instant 0.782 ms, 24 QC/Cs (i.e. $\lceil 0.75 \times 32 \rceil$) at time-instant 1.162 ms, 18 QC/Cs (i.e. $\lceil 0.75 \times 24 \rceil$) at time-instant 1.687 ms, 15 QC/Cs at time-instant 1.887 ms and 10 QC/Cs at time-instant 2.009 ms.

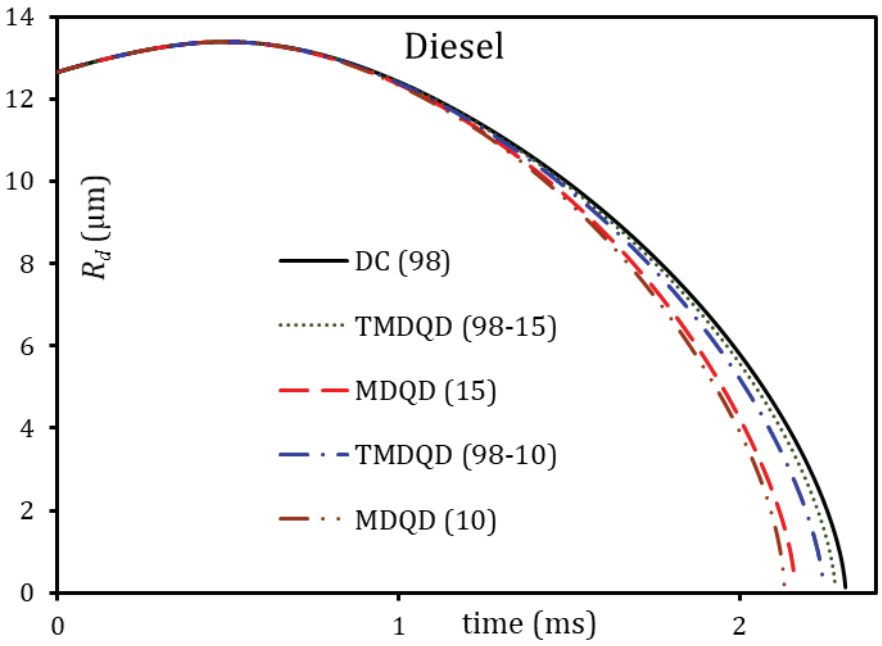

Figure 2. Evolutions of Diesel fuel (98 components) droplet radii versus time using the DC model, the original MDQD model and the new algorithm (TMDQD).

As can be seen in Figure 2, TMDQD 98-15 shows droplet radius evolution and lifetime nearest to those predicted using the DC model. This is followed by those predicted using TMDQD 98-10. The same trends are observed for droplet surface temperatures (see Figure 3).

It can be seen from Figures 2 and 3 that the evolutions of Diesel droplet radii and surface temperatures predicted using the new algorithm are almost identical to those predicted using the DC model at the earlier stages of evaporation. This can be attributed to the fact that the TMDQD algorithm starts with a higher number of QC/Cs (the full composition) compared with the

conventional MDQD model. The evolutions of blended Diesel-E85 fuel droplet radii and surface temperatures were investigated accounting for the contributions of all 119 components of E85-5 fuel blends, using the same algorithms as used for the plots in Figures 2 and 3. The results are presented in Figures 4 and 5.

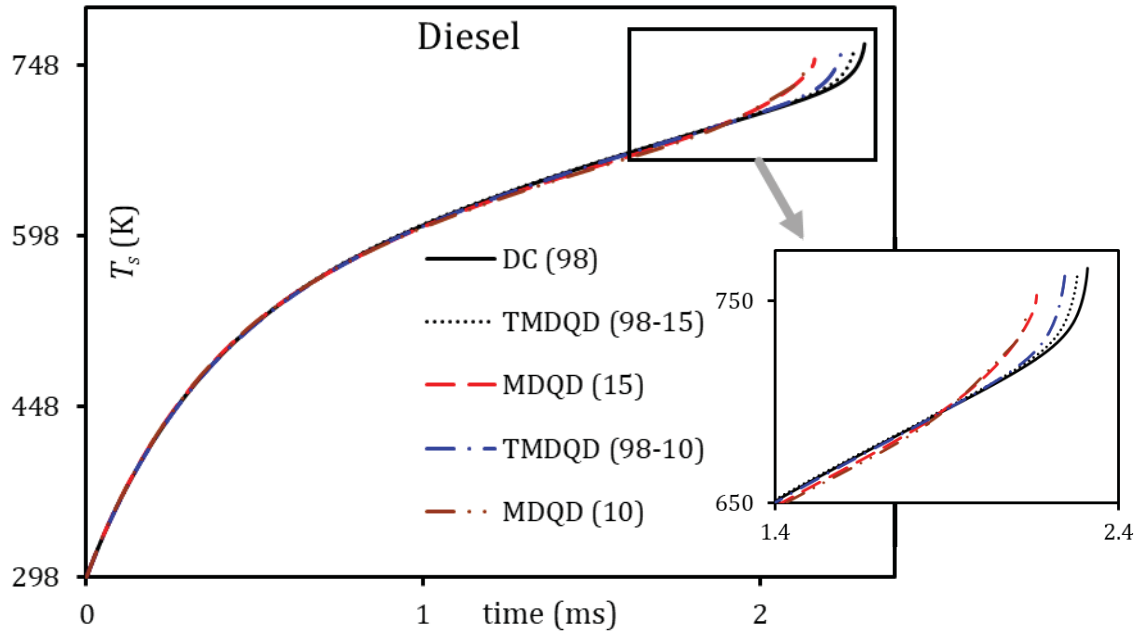

Figure 3. The same as Figure 2, but for droplet surface temperatures.

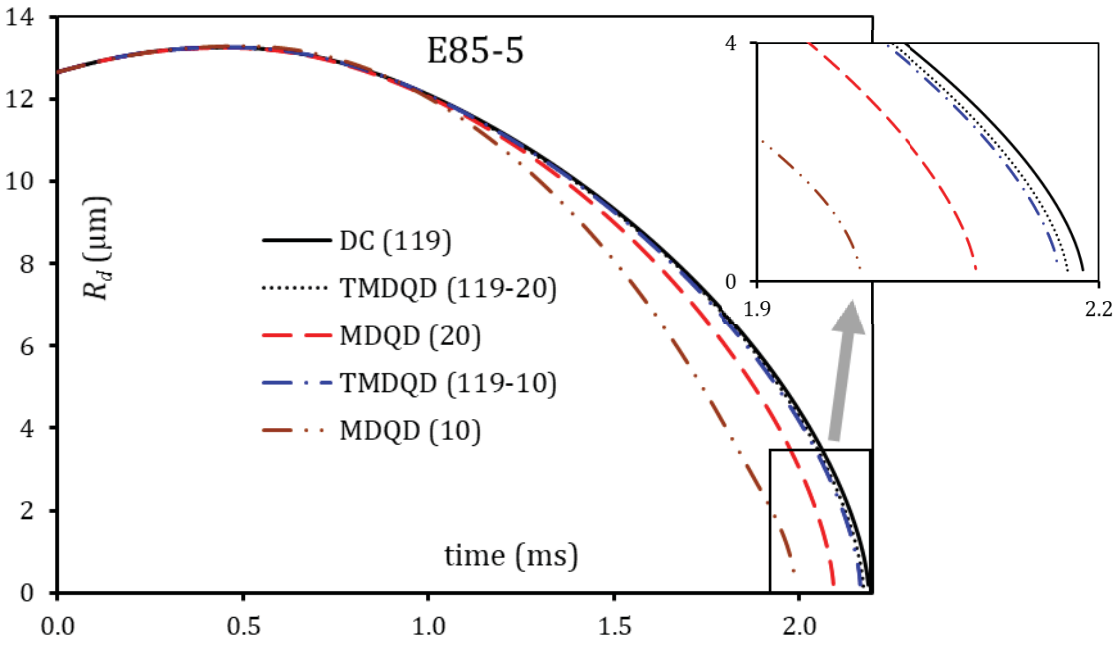

Figure 4. The same as Figure 2 but for E85-5 (95% Diesel and 5% E85) droplets.

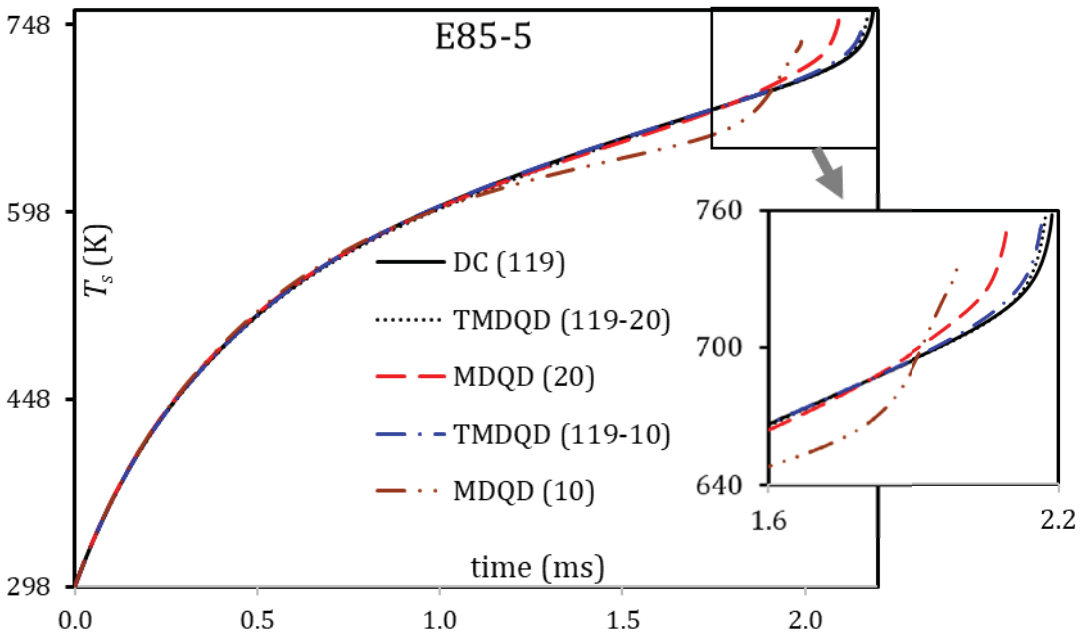

Figure 5. The same as Figure 3 but for E85-5 (95% Diesel and 5% E85) droplets.

As in the case of the pure Diesel fuel droplet (Figures 2 and 3), for the E85-5 fuel blend droplet, both the droplet lifetimes (Figure 4) and surface temperatures (Figure 5) predicted by the new algorithm are the closest to those predicted by the DC model. The predicted droplet lifetimes and evolutions of radii and surface temperatures of the other E85/Diesel fuel blends show the same trends as those presented in Figures 2–5. The predicted droplet lifetimes for several E85/Diesel fuel blends are presented in Table 3 and the corresponding plots are shown in Figures 6 and 7. In this table and these figures, the predictions of the original MDQD model, the new algorithm and the DC model are compared. An example of the detailed compositions of these blends, and the reduced components at various time instants is presented in Supplementary Material S1 for the E85-5 fuel blend.

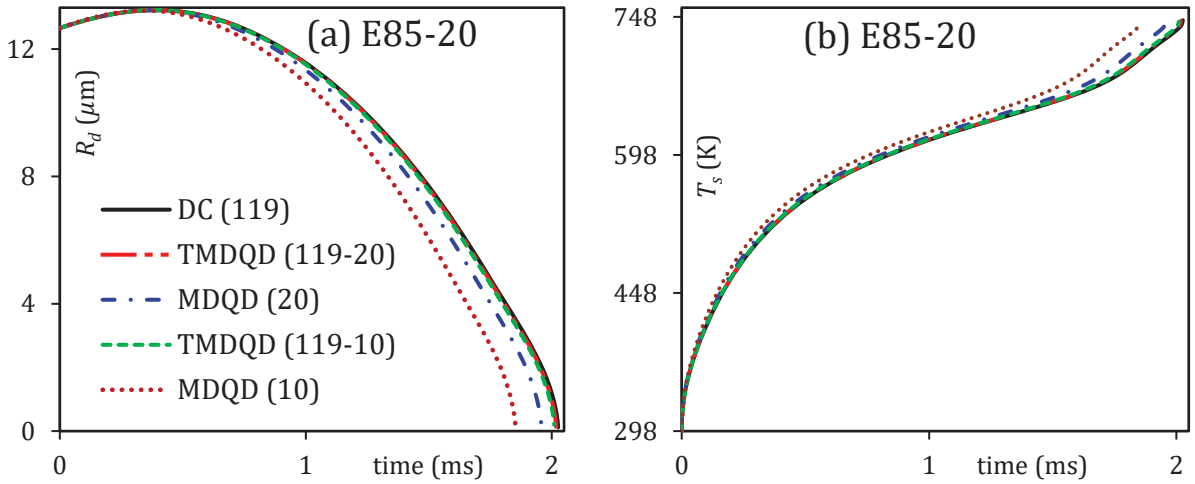

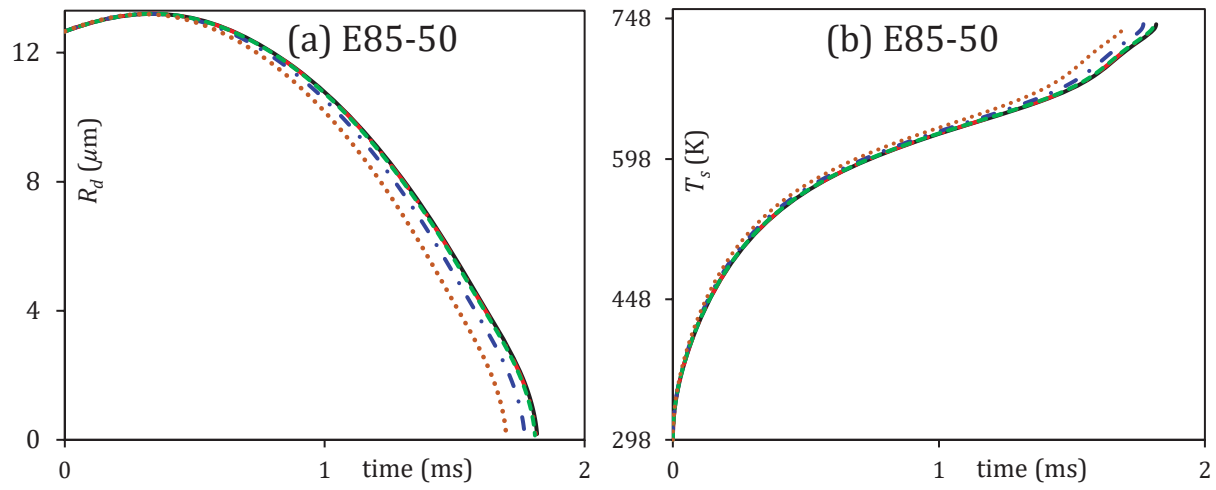

Figure 6. Evolutions of (a) droplet radii in μm and (b) surface temperatures in K versus time in ms for E85-20 and E85-50 fuel blends, using the DC (119 components), MDQD(20) (119 components are manually reduced to 20 QC/Cs), MDQD(10) (119 components are manually reduced to 10 QC/Cs), TMDQD(119-20) (119 components are auto-reduced to 20 QC/Cs), and TMDQD(119-10) (119 components are auto-reduced to 10 QC/Cs).

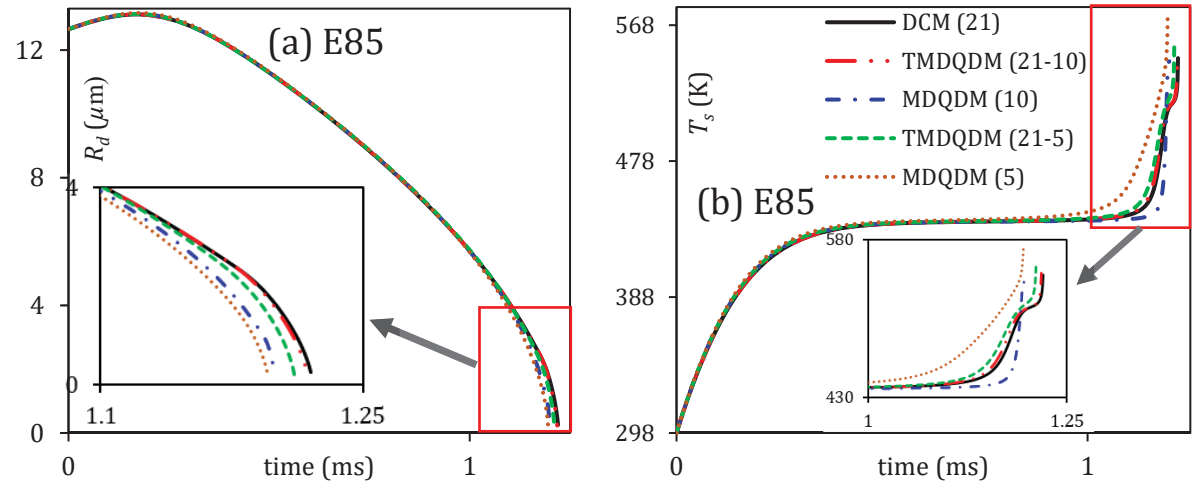

Figure 7. The same as Figure 6, but for E85 using the DC (21 components), MDQD(10) (21 components are manually reduced to 10 QC/Cs), MDQD(5) (21 components are manually reduced to 5 QC/Cs), TMDQD(21-10) (21 components are auto-reduced to 10 QC/Cs), and TMDQD(21-5) (21 components are auto-reduced to 5 QC/Cs).

Table 3. Droplet lifetimes (ms) for Diesel (98 components), E85/Diesel blends (119 components) and E85 (21 components) fuels, predicted by the TMDQD algorithm and the original MDQD model for 20, 10 and 5 QC/Cs. The errors in the predictions of TMDQD and MDQD are calculated relative to the

predictions of the DC model using parameter $\Delta\text{time} = (\text{time}_{\text{DC}} - \text{time}_{\text{model}}) \times 100\% \,/\text{time}_{\text{DC}}$, where time_{DC} is always greater than $\text{time}_{\text{model}}$.

Model	**Diesel**	Δtime	**E85-5**	Δtime	**E85-20**	Δtime	**E85-50**	Δtime	**E85**	Δtime
DC	2.310	0	2.186	0	2.026	0	1.817	0	1.220	0
TMDQD(20)	2.280	1.3	2.173	0.4	2.018	0.4	1.812	0.3	-	-
MDQD(20)	2.160	6.4	2.092	4.1	1.960	3.4	1.769	2.6	-	-
TMDQD (10)	2.246	2.8	2.164	0.8	2.010	0.8	1.809	0.4	1.218	0.2
MDQD(10)	2.130	7.8	1.990	8.8	1.850	8.6	1.698	6.6	1.990	1.2
TMDQD(5)	2.217	4.0	2.144	1.9	1.998	1.4	1.799	1.0	1.211	0.7
MDQD(5)	1.985	14.1	1.888	13.6	1.839	9.2	1.681	7.5	1.195	2.1

As can be seen in Table 3, the errors of predictions made by the MDQD model and TMDQD algorithm in most cases decrease, and the droplet lifetimes become shorter when the ratios of E85/Diesel increase. The general trends indicate noticeable improvement in the predictions of droplet lifetimes using the TMDQD algorithm, compared to the original MDQD model with 20, 10 and 5 QC/Cs. For example, reducing the 21 components of E85 fuel to 5 QC/Cs at the final stage of droplet evaporation, using this new algorithm, leads to underprediction of the droplet lifetime by up to 0.7%. In the case of the original MDQD model with 5 QC/Cs, this error increases to 2.1%. The processes preceding the onset of combustion (including physical autoignition delay) are typically 2– 6 ms within the idle speed range of all IC engines [37,38]; this can be shorter ($0.1 - 1.5$ ms) for rapid compression Diesel engines [39]. With such a short time, the accuracy of prediction of droplet lifetimes becomes particularly important. Hence, the application of the new algorithm for simulating these processes can be recommended for such conditions.

The values of droplet surface temperatures and radii versus the number of QC/Cs predicted using both versions of the MDQD based algorithms are shown in Figure 8. These results are estimated for the E85-5 fuel blend (inferred from [21,22]), composed of 119 components, at time instants $t = 0.3$ ms, $t = 0.5$ ms, $t = 1$ ms, $t = 1.5$ ms and $t = 2$ ms. The values of the numbers of QC/Cs used by the TMDQD algorithm were fixed at these time instants and are shown as triangles. Note that in the TMDQD algorithm the full composition of fuel is auto-reduced to different numbers of QC/Cs at different time instants. In the case of the original MDQD model, the number of QC/Cs is pre-defined for each separate code run.

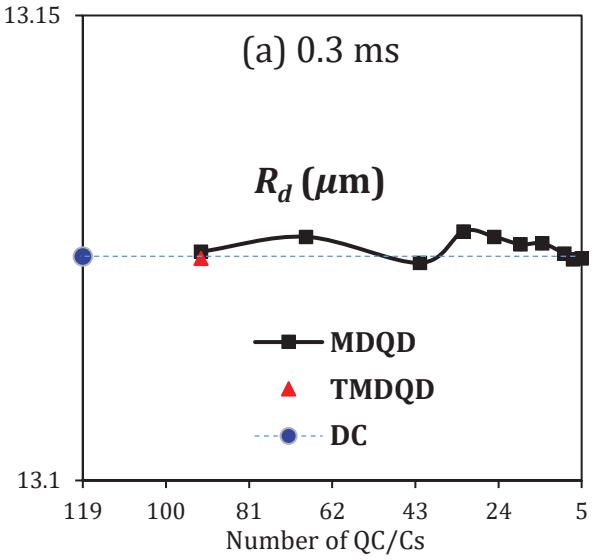
(a) 0.3 ms
R_d (μm)
13.15
13.1
MDQD
TMDQD
DC
119 100 81 62 43 24 5
Number of QC/Cs

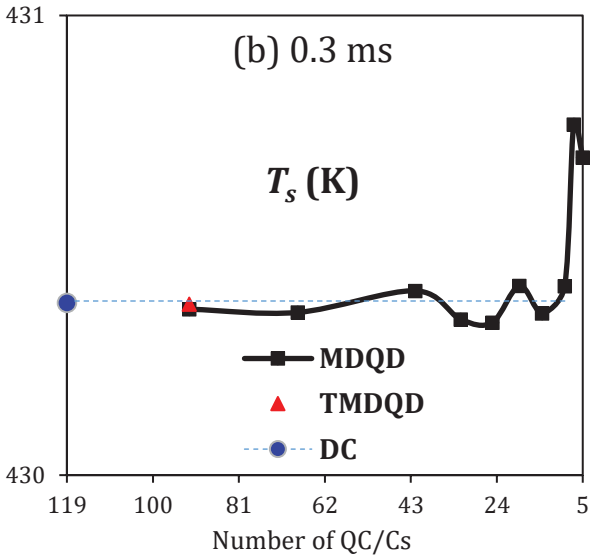
(b) 0.3 ms
T_s (K)
431
430
MDQD
TMDQD
DC
119 100 81 62 43 24 5
Number of QC/Cs

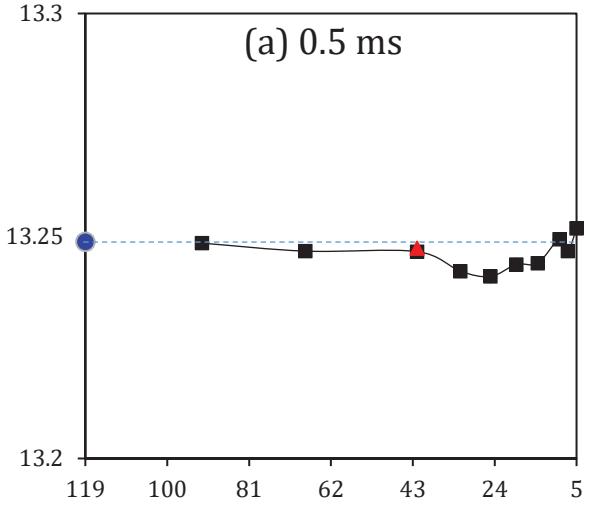
(a) 0.5 ms
13.3
13.25
13.2
119 100 81 62 43 24 5

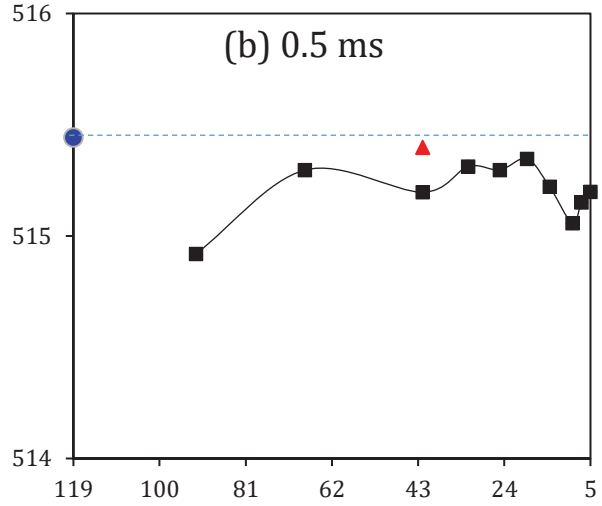
(b) 0.5 ms
516
515
514
119 100 81 62 43 24 5

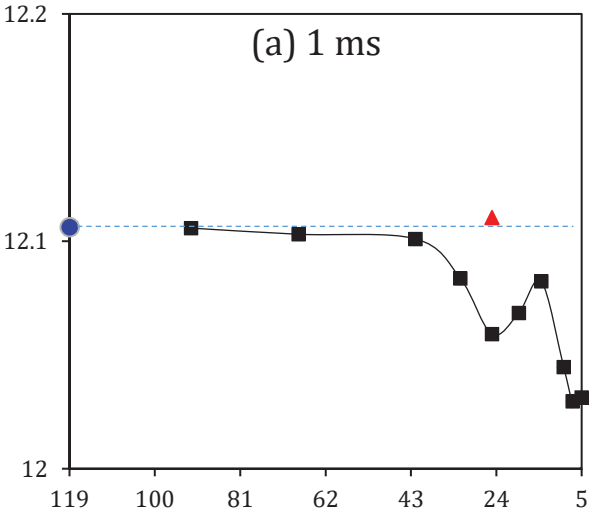
(a) 1 ms
12.2
12.1
12
119 100 81 62 43 24 5

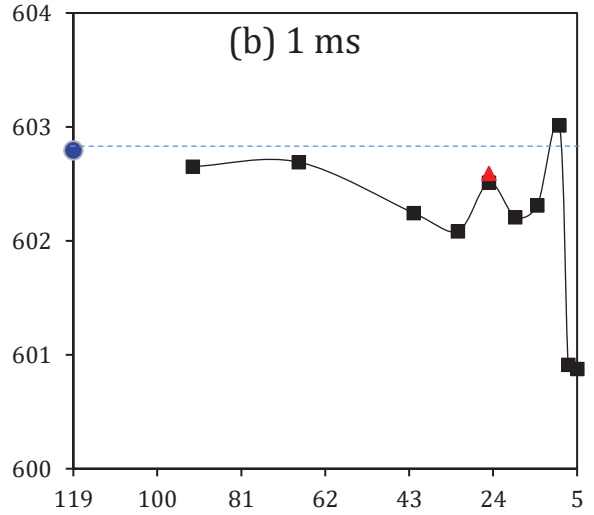
(b) 1 ms
604
603
602
601
600
119 100 81 62 43 24 5

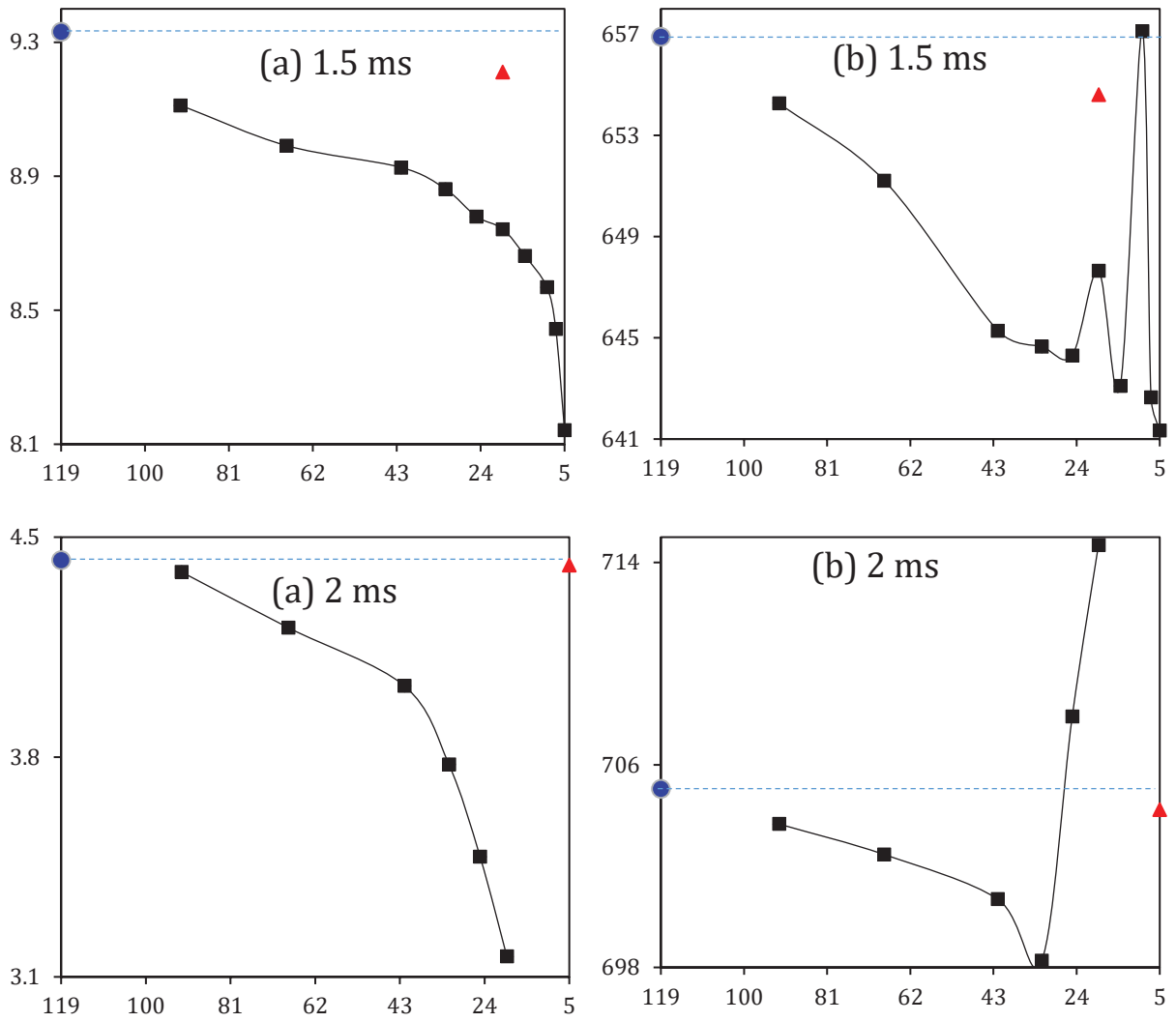

Figure 8. Droplet radii in μm (a) and surface temperatures in K (b) versus the numbers of QC/Cs predicted by the TMDQD algorithm (▲), the DC model (●) and the original MDQD model (■) at time instants (0.3 ms, 0.5 ms, 1 ms, 1.5 ms and 2 ms) for various numbers of QC/Cs, using the same parameters as in Figures 2-5.

As can be seen from Figure 8, the predictions of the TMDQD algorithm for droplet surface temperatures and radii are generally more consistent with the DC model predictions than those predicted using the original MDQD model. Note that the predictions of both approaches are closer at the early stages of heating and evaporation (up to 0.5 ms) than at the later times. As in [4,20], the predictions of the original MDQD model show fluctuations in droplet radii and surface temperatures for small numbers of QC/Cs. This is attributed to the fact that the reduction in the number of QC/Cs in the original MDQD model is based on trial-and-error, which requires experienced end-users and makes it difficult to implement this approach into CFD codes. Note that the fluctuations predicted by the original MDQD model become less visible at later evaporation times (≥ 1 ms), when the lighter (volatile) components have mostly evaporated. At times close to the evaporation time (>1.5 ms), the original MDQD model fails to predict the droplet surface temperatures and radii accurately. The deviation becomes more noticeable for small numbers of QC/Cs in the MDQD.

The time evolution of mass fractions of selected species at the surface of an E85-5 fuel droplet, predicted by the DC model, is shown in Figure 9. These are typical examples of the evolutions of heavy, intermediate and light species of the initial 119 components in the E85-Diesel fuel blend.

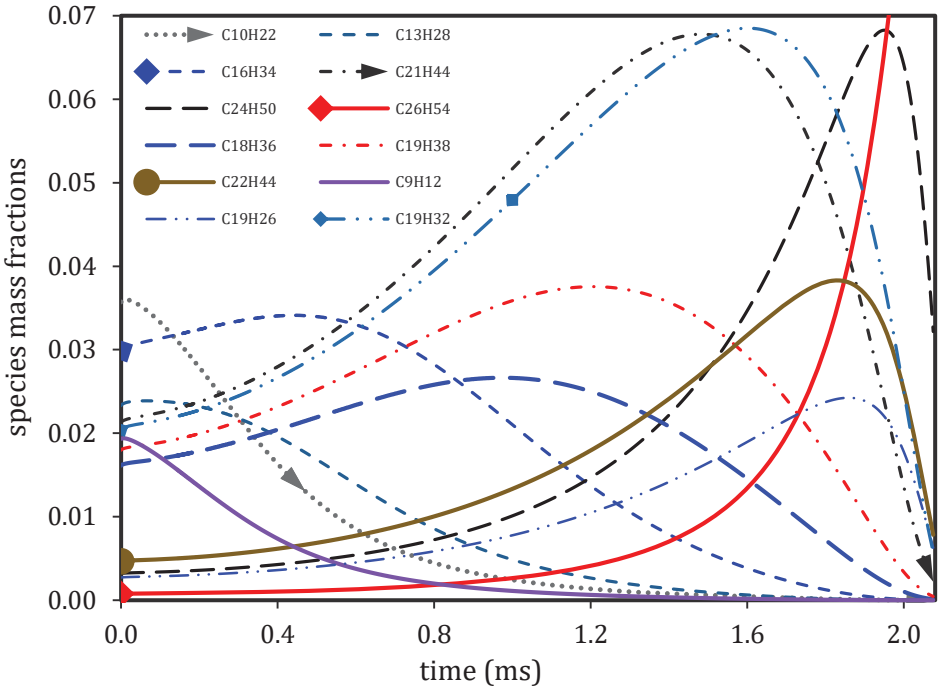

Figure 9. Liquid mass fractions of species at the surface of an E85-5 fuel droplet versus time for the same conditions as in Figures 4-7.

As follows from Figure 9, the evolutions of mass fractions of species at the surface of the droplet show trends similar to those observed for Diesel, gasoline and biodiesel fuels [4,23]. The heavy components ($C_{24}H_{50}, C_{26}H_{54}$) gradually dominate the droplet composition at the expense of the light ones ($C_9H_{12}, C_{10}H_{22}$), while the intermediate species ($C_{16}H_{34}, C_{19}H_{38}$) first increase and then decrease at later stages of droplet heating and evaporation. Also, the heavy species tend to evaporate more slowly than the lighter ones, due to their lower saturation vapour pressures. The CPU times required to run calculations and errors, using different models, for an E85-Diesel fuel blend are presented in Figure 10 and Table 4.

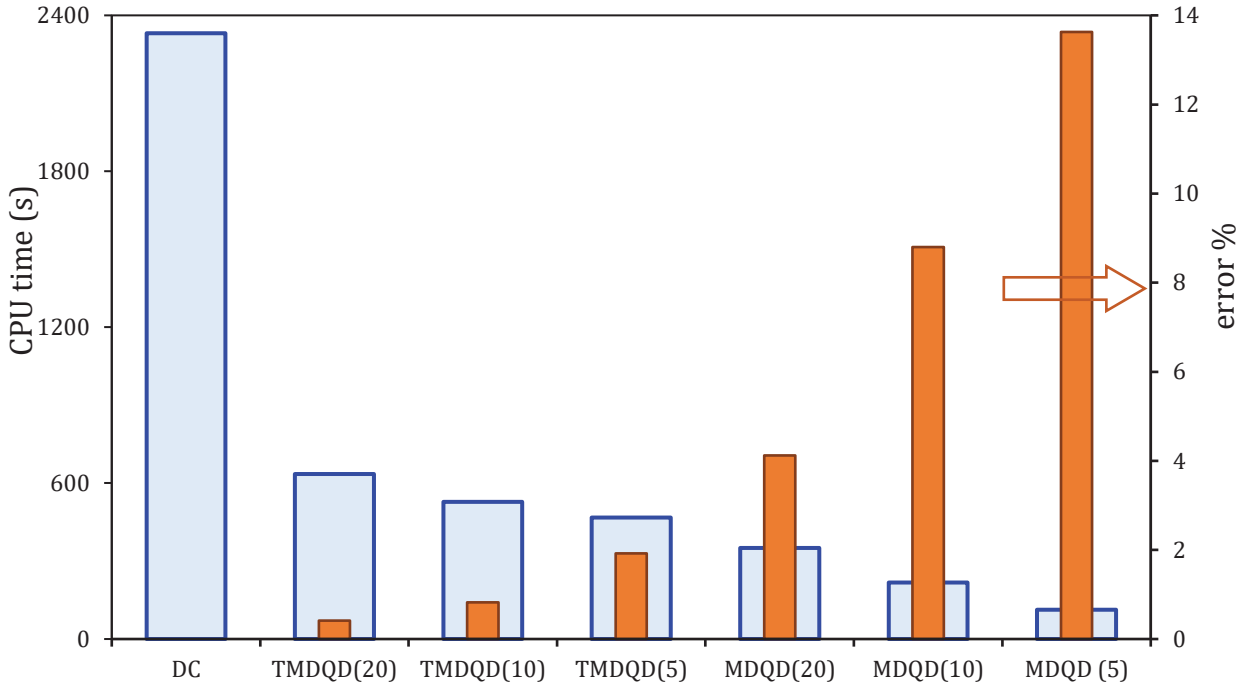

Figure 10. CPU times (wide bars) and errors (narrow bars) for six modelling approaches, compared with the predictions of the DC model for an E85-5 fuel blend. The errors are calculated as error% = $(\text{time}_{DC} - \text{time}_{model}) \times 100\%/\text{time}_{DC}$, where time_{DC} is always greater than time_{model}. The full composition of an E85-5 fuel blend (119 components) is auto-reduced to 20, 10 and 5 QC/Cs using the TMDQD algorithm, indicated as TMDQD(20), TMDQD(10), TMDQD(5), respectively, and the same composition is reduced to 20, 10 and 5 QC/Cs using the original MDQD model, indicated as MDQD(20), MDQD(10) and MDQD(5), respectively.

Table 4. CPU time (in s) required for TDMDQ and MDQD model calculations for Diesel fuel or its blends (first columns), and the time saving compared to the DC model, calculated as $T.S.\% = (CPU_{DC} - CPU_{model}) \times 100\% / CPU_{DC}$ (second columns). The workstation used was fitted with an i7-3337U core, 4 GB RAM, and a 2.0 GHz processor. The time-step was set as 1 μs. An example of the detailed compositions of E85-5 during the reduction of QC/Cs predicted by TMDQD(5) is shown in Supplementary Material S1.

Model	**CPU time (s) and time savings (T.S.%) compared to DCM**									
	Diesel	**T.S.%**	**E85-5**	**T.S.%**	**E85-20**	**T.S.%**	**E85-50**	**T.S.%**	**E85**	**T.S.%**
DC	2511	-	2331	-	2177	-	1985	-	306	-
TMDQD(20)	789	68.6	635	72.8	537	75.3	488	75.42	-	-
MDQD(20)	428	82.9	351	84.9	427	80.4	363	81.71	-	-
TMDQD(10)	698	72.2	528	77.4	480	77.95	421	78.79	158	48.40
MDQD(10)	329	86.9	218	90.7	306	85.94	261	86.85	107	65.03
TMDQD(5)	621	75.3	467	80.0	472	78.32	396	80.03	141	53.92
MDQD (5)	140	94.4	113	95.2	110	94.9	103	94.80	79	74.18

As can be seen from Figure 10 and Table 4, there is a noticeable improvement in the predictions of the MDQD model with the new algorithm (TMDQD) compared to the same predictions made using the original MDQD model with fixed numbers of QC/Cs, but at the expense of computational time.

This is attributed to the fact that the new algorithm starts with higher numbers of QC/Cs than those used in the original MDQD model. For example, the approximation of all 119 components of an E85-5 fuel blend by 10 QC/Cs using the original MDQD model saves up to 90.7% of CPU time, and using the TMDQD model saves up to 77.4% of CPU time. The approximation of the same blend by 5 QC/Cs saves up to 95.2% and 80%, respectively, using the original MDQD and TMDQD models. The new algorithm can be considered a compromise between the DC and MDQD models for wider engineering applications where both accuracy and CPU efficiency are needed.

6. Conclusion

A new approach for calculating multi-component fuel droplet heating and evaporation based on the previously developed multi-dimensional quasi-discrete (MDQD) model is suggested. As in the original MDQD model, a large number of fuel components is reduced to a much smaller number of components and quasi-components. In contrast to the original MDQD model, in the new approach the number of quasi-components/components is not fixed during the whole process but is automatically reduced when the droplet evaporates. The new approach is called the transient multi-dimensional quasi-discrete (TMDQD) algorithm. This algorithm is applied to a wide range of E85 (85% ethanol and 15% gasoline) and Diesel fuel blends (E85, E85-5, E85-20, E85-50) and pure Diesel.

It is shown that using the TMDQD algorithm allows us to reduce the full compositions of E85-Diesel mixtures from their initial 119 components to 5 quasi-components/components at the end of the heating and evaporation process with less than 1.9% errors in predicted droplet lifetimes and temperatures. These predictions are shown to be more accurate than those obtained using the original version of the MDQD model. The CPU time needed to run this algorithm is 80% less than that needed by the Discrete Component (DC) model using the full composition of fuel.

Acknowledgement

The authors are grateful to the Institute for Future Transport and Cities, Coventry University, UK (Project Ref. ECR019) (M.A., N.A.) and EPSRC, UK (Grant no. EP/M002608/1) (S.S.S.) for their financial support.

References

[1] Wang J, Huang X, Qiao X, Ju D, Sun C. Experimental study on evaporation characteristics of single and multiple fuel droplets. J Energy Inst 2020;93:1473–80. https://doi.org/10.1016/j.joei.2020.01.009.
[2] Sirignano WA. Fluid Dynamics and Transport of Droplets and Sprays. Cambridge, U.K: Cambridge University Press; 1999.
[3] Divis M, Tiney NK, Lucas G. Spray Modeling of Multicomponent Fuels in Industrial Time Frames Using 3D CFD. In: Liebl J, Beidl C, editors. VPC – Simul. Test 2016, Wiesbaden: Springer Fachmedien Wiesbaden; 2017, p. 132–52. https://doi.org/10.1007/978-3-658-16754-7_9.
[4] Sazhin SS, Al Qubeissi M, Nasiri R, Gun'ko VM, Elwardany AE, Lemoine F, et al. A multi-dimensional quasi-discrete model for the analysis of Diesel fuel droplet heating and evaporation. Fuel 2014;129:238–66. https://doi.org/10.1016/j.fuel.2014.03.028.
[5] Sazhin SS. Droplets and Sprays. London: Springer; 2014.

[6] Sazhin SS. Modelling of fuel droplet heating and evaporation: Recent results and unsolved problems. Fuel 2017;196:69–101. https://doi.org/10.1016/j.fuel.2017.01.048.
[7] Abramzon B, Sirignano WA. Droplet vaporization model for spray combustion calculations. Int J Heat Mass Transf 1989;32:1605–18. https://doi.org/10.1016/0017-9310(89)90043-4.
[8] Al-Esawi N, Al Qubeissi M, Sazhin SS. The impact of fuel blends and ambient conditions on the heating and evaporation of Diesel and biodiesel fuel droplets. Int. Heat Transf. Conf. 16, Beijing, China: Begellhouse; 2018, p. 6641–8. https://doi.org/10.1615/IHTC16.mpf.020772.
[9] Castanet G, Frackowiak B, Tropea C, Lemoine F. Heat convection within evaporating droplets in strong aerodynamic interactions. Int J Heat Mass Transf 2011;54:3267–76. https://doi.org/10.1016/j.ijheatmasstransfer.2011.03.060.
[10] Saggese C, Singh AV, Xue X, Chu C, Kholghy MR, Zhang T, et al. The distillation curve and sooting propensity of a typical jet fuel. Fuel 2019;235:350–62. https://doi.org/10.1016/j.fuel.2018.07.099.
[11] Kitano T, Nishio J, Kurose R, Komori S. Effects of ambient pressure, gas temperature and combustion reaction on droplet evaporation. Combust Flame 2014;161:551–64. https://doi.org/10.1016/j.combustflame.2013.09.009.
[12] Ali OM, Mamat R, Abdullah NR, Abdullah AA. Analysis of blended fuel properties and engine performance with palm biodiesel–diesel blended fuel. Renew Energy 2016;86:59–67. https://doi.org/10.1016/j.renene.2015.07.103.
[13] An H, Yang WM, Maghbouli A, Chou SK, Chua KJ. Detailed physical properties prediction of pure methyl esters for biodiesel combustion modeling. Appl Energy 2013;102:647–56. https://doi.org/10.1016/j.apenergy.2012.08.009.
[14] Sazhin SS, Al Qubeissi M, Xie J-F. Two approaches to modelling the heating of evaporating droplets. Int Commun Heat Mass Transf 2014;57:353–6. https://doi.org/10.1016/j.icheatmasstransfer.2014.08.004.
[15] Sazhin SS, Al Qubeissi M, Kolodnytska R, Elwardany AE, Nasiri R, Heikal MR. Modelling of biodiesel fuel droplet heating and evaporation. Fuel 2014;115:559–72. https://doi.org/10.1016/j.fuel.2013.07.031.
[16] Poulton L, Rybdylova O, Zubrilin IA, Matveev SG, Gurakov NI, Al Qubeissi M, et al. Modelling of multi-component kerosene and surrogate fuel droplet heating and evaporation characteristics: A comparative analysis. Fuel 2020;269:117115. https://doi.org/10.1016/j.fuel.2020.117115.
[17] Al-Esawi N, Al Qubeissi M, Kolodnytska R. The Impact of Biodiesel Fuel on Ethanol/Diesel Blends. Energies 2019;12:1804. https://doi.org/10.3390/en12091804.
[18] Rybdylova O, Poulton L, Al Qubeissi M, Elwardany AE, Crua C, Khan T, et al. A model for multi-component droplet heating and evaporation and its implementation into ANSYS Fluent. Int Commun Heat Mass Transf 2018;90:29–33. https://doi.org/10.1016/j.icheatmasstransfer.2017.10.018.
[19] Sazhin SS, Elwardany AE, Sazhina EM, Heikal MR. A quasi-discrete model for heating and evaporation of complex multicomponent hydrocarbon fuel droplets. Int J Heat Mass Transf 2011;54:4325–32. https://doi.org/10.1016/j.ijheatmasstransfer.2011.05.012.
[20] Al Qubeissi M. Predictions of droplet heating and evaporation: an application to biodiesel, diesel, gasoline and blended fuels. Appl Therm Eng 2018;136:260–7. https://doi.org/10.1016/j.applthermaleng.2018.03.010.
[21] Al-Esawi N, Al Qubeissi M, Whitaker R, Sazhin SS. Blended E85–Diesel Fuel Droplet Heating and Evaporation. Energy Fuels 2019;33:2477–88. https://doi.org/10.1021/acs.energyfuels.8b03014.
[22] Al Qubeissi M, Al-Esawi N, Sazhin SS, Ghaleeh M. Ethanol/Gasoline Droplet Heating and Evaporation: Effects of Fuel Blends and Ambient Conditions. Energy Fuels 2018;32:6498–506. https://doi.org/10.1021/acs.energyfuels.8b00366.
[23] Al Qubeissi M, Sazhin SS, Turner J, Begg S, Crua C, Heikal MR. Modelling of gasoline fuel droplets heating and evaporation. Fuel 2015;159:373–84. https://doi.org/10.1016/j.fuel.2015.06.028.
[24] Al Qubeissi M, Sazhin SS, Elwardany AE. Modelling of blended Diesel and biodiesel fuel droplet heating and evaporation. Fuel 2017;187:349–55. https://doi.org/10.1016/j.fuel.2016.09.060.
[25] Al-Esawi N, Al Qubeissi M. A new approach to formulation of complex fuel surrogates. Fuel 2021;283:118923. https://doi.org/10.1016/j.fuel.2020.118923.
[26] Sazhin SS. Advanced models of fuel droplet heating and evaporation. Prog Energy Combust Sci 2006;32:162–214. https://doi.org/10.1016/j.pecs.2005.11.001.
[27] Al Qubeissi M. Heating and Evaporation of Multi-Component Fuel Droplets. Stuttgart: WiSa; 2015.
[28] Sazhin SS, Krutitskii PA, Abdelghaffar WA, Sazhina EM, Mikhalovsky SV, Meikle ST, et al. Transient heating of diesel fuel droplets. Int J Heat Mass Transf 2004;47:3327–40. https://doi.org/10.1016/j.ijheatmasstransfer.2004.01.011.
[29] Sazhin SS, Elwardany A, Krutitskii PA, Castanet G, Lemoine F, Sazhina EM, et al. A simplified model for bi-component droplet heating and evaporation. Int J Heat Mass Transf 2010;53:4495–505. https://doi.org/10.1016/j.ijheatmasstransfer.2010.06.044.
[30] Elwardany AE, Gusev IG, Castanet G, Lemoine F, Sazhin SS. Mono- and multi-component droplet cooling/heating and evaporation: comparative analysis of numerical models. At Sprays 2011;21:907–31. https://doi.org/10.1615/AtomizSpr.2012004194.

[31] Sazhin SS, Elwardany AE, Krutitskii PA, Deprédurand V, Castanet G, Lemoine F, et al. Multi-component droplet heating and evaporation: Numerical simulation versus experimental data. Int J Therm Sci 2011;50:1164–80. https://doi.org/10.1016/j.ijthermalsci.2011.02.020.
[32] Al-Esawi N, Al Qubeissi M, Sazhin SS, Whitaker R. The impacts of the activity coefficient on heating and evaporation of ethanol/gasoline fuel blends. Int Commun Heat Mass Transf 2018;98:177–82. https://doi.org/10.1016/j.icheatmasstransfer.2018.08.018.
[33] Poling BE, Prausnitz JM, O'Connell JP. The properties of gases and liquids. New York: McGraw-Hill; 2001.
[34] Reid RC, Prausnitz JM, Poling BE. The properties of gases and liquids. 4th ed. New York: McGraw-Hill; 1987.
[35] Kwanchareon P, Luengnaruemitchai A, Jai-In S. Solubility of a diesel–biodiesel–ethanol blend, its fuel properties, and its emission characteristics from diesel engine. Fuel 2007;86:1053–61. https://doi.org/10.1016/j.fuel.2006.09.034.
[36] Satgé de Caro P. Interest of combining an additive with diesel–ethanol blends for use in diesel engines. Fuel 2001;80:565–74. https://doi.org/10.1016/S0016-2361(00)00117-4.
[37] Efthymiou P, Davy MH, Garner CP, Hargrave GK, Rimmer JET, Richardson D, et al. An optical investigation of a cold-start DISI engine startup strategy. Intern. Combust. Engines Perform. Fuel Econ. Emiss., Elsevier; 2013, p. 33–52. https://doi.org/10.1533/9781782421849.1.33.
[38] Petrukhin NV, Grishin NN, Sergeev SM. Ignition Delay Time – an Important Fuel Property. Chem Technol Fuels Oils 2016;51:581–4. https://doi.org/10.1007/s10553-016-0642-0.
[39] Kobori S, Kamimoto T, Aradi AA. A study of ignition delay of diesel fuel sprays. Int J Engine Res 2000;1:29–39. https://doi.org/10.1243/1468087001545245.